Received: 12 April 2024 | Revised: 12 July 2024 | Accepted: 16 July 2024

DOI: 10.1002/alz.14176

Alzheimer's & Dementia®
THE JOURNAL OF THE ALZHEIMER'S ASSOCIATION

RESEARCH ARTICLE

Spatial and temporal patterns of cortical mean diffusivity in Alzheimer's disease and suspected non-Alzheimer's disease pathophysiology

Pan Sun[1,2] | **Zhengbo He**[1] | **Anqi Li**[1] | **Jie Yang**[1] | **Yalin Zhu**[1] | **Yue Cai**[1] | **Ting Ma**[3] | **Shaohua Ma**[2] | **Tengfei Guo**[1,4] | **Alzheimer's Disease Neuroimaging Initiative**

[1]Institute of Biomedical Engineering, Shenzhen Bay Laboratory, Shenzhen, China

[2]Tsinghua Shenzhen International Graduate School (SIGS), Tsinghua University, Shenzhen, China

[3]School of Electronic and Information Engineering, Harbin Institute of Technology (Shenzhen), Shenzhen, China

[4]Institute of Biomedical Engineering, Peking University Shenzhen Graduate School, Shenzhen, China

Correspondence
Tengfei Guo, Institute of Biomedical Engineering, Shenzhen Bay Laboratory, No.5 Kelian Road, Shenzhen, 518132, China.
Email: tengfei.guo@pku.edu.cn

† Data used in preparation of this article were obtained from the Alzheimer's Disease Neuroimaging Initiative (ADNI) database (adni.loni.usc.edu). As such, the investigators within the ADNI contributed to the design and implementation of ADNI and/or provided data but did not participate in the analysis or writing of this report. A complete listing of ADNI investigators can be found at: http://adni.loni.usc.edu/wp-content/uploads/how_to_apply/ADNI_Acknowledgement_List.pdf.

Funding information
the Guangdong Basic and Applied Basic Science Foundation for Distinguished Young Scholars, Grant/Award Number: 2023B1515020113; the Shenzhen Science and Technology Program, Grant/Award Number: RCYX20221008092935096; National Natural Science Foundation of China, Grant/Award Number: 82171197; Shenzhen Bay Laboratory, Grant/Award Numbers: S241101004-1, 21300061; the Lingang Laboratory, Grant/Award Number: LG-GG-202401-ADA070600

Abstract

INTRODUCTION: The spatial and temporal patterns of cortical mean diffusivity (cMD), as well as its association with Alzheimer's disease (AD) and suspected non-Alzheimer's pathophysiology (SNAP), are not yet fully understood.

METHODS: We compared baseline (n = 617) and longitudinal changes (n = 421) of cMD, cortical thickness, and gray matter volume and their relations to vascular risk factors, amyloid beta (Aβ), and tau positron emission tomography (PET), and longitudinal cognitive decline in Aβ PET negative and positive older adults.

RESULTS: cMD increases were more sensitive to detecting brain structural alterations than cortical thinning and gray matter atrophy. Tau-related cMD increases partially mediated Aβ-related cognitive decline in AD, whereas vascular disease-related increased cMD levels substantially mediated age-related cognitive decline in SNAP.

DISCUSSION: These findings revealed the dynamic changes of microstructural and macrostructural indicators and their associations with AD and SNAP, providing novel insights into understanding upstream and downstream events of cMD in neurodegenerative disease.

KEYWORDS
age, Alzheimer's disease, cortical mean diffusivity, suspected non-Alzheimer's pathophysiology, vascular disease

Highlights

- Cortical mean diffusivity (cMD) was more sensitive to detecting structural changes than macrostructural factors.
- Tau-related cMD increases partially mediated amyloid beta–related cognitive decline in Alzheimer's disease (AD).
- White matter hyperintensity–related higher cMD mainly explained the age-related cognitive decline in suspected non-Alzheimer's pathophysiology (SNAP).
- cMD may assist in tracking earlier neurodegenerative signs in AD and SNAP.

1 | BACKGROUND

Aggregation of extracellular amyloid beta (Aβ) plaques and intracellular neurofibrillary tau tangles (NFTs) are two core features of Alzheimer's disease (AD).[1] Positron emission tomography (PET) imaging of Aβ and tau is commonly used as a proxy for evaluating Aβ plaques and tau tangles in AD.[2,3] According to the biological definition of AD, individuals with substantial Aβ pathology positive (A+) are considered on the AD continuum,[4] whereas individuals with abnormal tau or neurodegeneration but normal Aβ pathology are defined as suspected non-Alzheimer's pathophysiology (SNAP).[5] Critically, AD and SNAP patients may have Aβ-related and non-Aβ-related downstream events, respectively, such as tau aggregation, brain structural dysfunction, and cognitive decline.[6–15]

Diffusion-weighted imaging (DWI) could probe the microstructural properties of tissue by investigating the random displacement of water molecules in presymptomatic familial AD.[16] Although most studies have used DWI to assess microstructural alterations in white matter, a growing amount of evidence suggests that cortical mean diffusivity (cMD) could also capture the microstructurally isotropic changes in the gray matter in AD and non-AD diseases.[17,18] Specifically, it has been hypothesized that cMD may have a biphasic trajectory along AD progression in both sporadic AD[19] and autosomal dominant AD,[20] indicating that cMD initially decreases along with Aβ deposition, astrocytosis, or inflammatory response, followed by cMD increases probably due to the breakdown of microstructural barriers. Increases in cMD have been observed in frontotemporal dementia (FTD) and amyotrophic lateral sclerosis (ALS),[18] and other dementias[21] as well. Meanwhile, regionally elevated cMD could predict longitudinal hippocampal atrophy and cognitive decline independent of Aβ, tau, and cortical thickness.[22] Mean diffusivity (MD) is frequently found vulnerable with age[23] and vascular disease[24] in white matter. However, in gray matter, we do not fully understood the dynamic changes of cMD as well as how it relates to age, vascular disease, Aβ, tau, brain atrophy, cortical thinning, and cognitive decline in Aβ negative (A–), and A+ older adults. Moreover, whether the cMD is more sensitive to detecting earlier abnormal structural changes in the brain than cortical thickness (CTh) and gray matter volume (GMV) in neurodegenerative disease remains to be further investigated.

In this study, we analyzed the baseline and longitudinal changes of cMD, CTh, and GMV based on the diffusion and 3D T1-weighted magnetic resonance imaging (MRI) images from the Alzheimer's Disease Neuroimaging Initiative (ADNI) cohort, aiming to investigate the cross-sectional and longitudinal characteristics of cMD, CTh, and GMV as well as how they correlate with age, vascular disease, Aβ, tau, and cognitive decline in A– cognitively unimpaired (CU), A+/CU, A– cognitively impaired (CI), and A+/CI individuals. Ultimately, we want to determine how cross-sectional and longitudinal cMD correlate with age, vascular risk factors, Aβ plaque, and tau tangles and whether cMD can detect more robust structural changes compared to the AD-signature[25] CTh and GMV changes in AD and SNAP individuals.

2 | METHODS

2.1 | Participants

Data used in this study were obtained from the ADNI (https://adni.loni.usc.edu/), which was launched in 2003 led by Principal Investigator Michael W. Weiner, MD. As a public–private partnership, the main objective of ADNI is to measure the progression of mild cognitive impairment (MCI) and early AD by combining serial MRI, PET, clinical and neuropsychological assessment, and biological and genetic biomarkers. The ADNI study was approved by institutional review boards of all participating institutions, and written informed consent was obtained for ethical considerations.

In this study, we identified 617 ADNI participants who had baseline Aβ PET (^{18}F-florbetapir [FBP] or ^{18}F-florbetaben [FBB]) and concurrent (within 1 year) DWI (single-shell or multi-shell), anatomical 3D T1 MRI, and cognitive assessment, of which 382 individuals had tau PET (^{18}F-flortaucipir [FTP]). MCI and dementia patients were merged into the CI group. Longitudinally, 421 individuals had at least one follow-up DWI and 3D T2 fluid-attenuated inversion recovery (FLAIR) MRI image scan, of which 195 were CU and 226 were CI individuals. Two hundred twenty-one individuals had tau PET with at least one simultaneous DWI and T2 FLAIR MRI scan, including 118 CU and 93 CI participants.

2.2 | MR imaging and analysis

Details on T1, T2 FLAIR, and DWI scan acquisition are given elsewhere (https://adni.loni.usc.edu/). In brief, the ADNI T1 MRI scans were acquired with a sagittal 3D accelerated magnetization-prepared rapid gradient-echo (MPRAGE) or inversion-recovery spoiled gradient-echo (IR-SPGR) sequence on the same date as the 3D T2 FLAIR, and axial DWI with an echo planar imaging sequence. Notably, in the third phase of ADNI, the multi-shell DWI protocol was scanned in a subset of participants.

The T1 images were processed using FreeSurfer (v. 7.2.0), which provided automatic preprocessing steps for motion correction, intensity normalization, removal of non-brain tissue, subcortical segmentation, and cortical parcellation. GMV was obtained, and CTh was estimated as the distance from the gray/white matter boundary to the corresponding pial surface.

A detailed description of T2 FLAIR segmentation and white matter hyperintensity (WMH) volume calculation was published previously.[26] Briefly, after co-registering the T2 FLAIR image to the FreeSurfer-processed T1 image, an anatomical-based MRI deep learning model was used with the T2 FLAIR image as the input, and then a binary WMH was obtained. The resulting WMH mask was further corrected for false positives in the choroid plexus of the lateral ventricle based on the cerebrospinal fluid (CSF) mask and was manually edited by two senior physicians to ensure consistency and accuracy. Finally, the total WMH value was calculated, and log transformation was applied to meet the normalization.

The raw DWI data were processed using open-source algorithms from MRTrix3 (v. 3.0.3), FSL (v. 6.0.3), and Advanced Normalization Tools (ANTs, v. 2.4.3). Specifically, pre-processing of the diffusion data included denoising based on Marchenko–Pastur principal component analysis (MP-PCA), Gibbs ringing removal, eddy current-induced distortions, motion correction, and B1 field inhomogeneity correction. After removing non-brain tissue using the Brain Extraction Tool (BET), the diffusion tensor imaging (DTI) model was fitted to compute the MD metric using FSL. Notably, for the multi-shell DWI data, volumes with a b-value of 1000 s/mm^2 were used to fit the DTI model. We then co-registered the averaged b0 image to the corresponding skull-tripped 3D T1 using a boundary-based algorithm and warped the MD metric. A surface-based approach was adopted to mitigate partial volume correction (PVC) and kernel-sensitive CSF signal inclusion. Briefly, the volume MD metric for each participant was sampled at the midpoint of the cortical ribbon and projected to each cortical surface obtained during the FreeSurfer step to create a surface map of the cMD. Finally, the individual cMD was smoothed using a 15 mm full width at half maximum (FWHM) Gaussian kernel. Visual quality control was inspected for the raw DWI scan and processed image.

The averaged cMD, CTh, and GMV values were extracted from the 68 FreeSurfer regions of interest (ROIs) defined by the Desikan–Killiany atlas based on processed DWI and FreeSurfer segmented anatomical 3D T1 MRI. CTh and GMV in AD-signature temporal-metaROI,[25] including entorhinal, inferior temporal, middle temporal, and fusiform regions, were calculated using surface-area weighted average or volume-weighted summation.

RESEARCH IN CONTEXT

1. **Systematic review**: Literature reviews in PubMed and Google Scholar suggest cortical mean diffusivity (cMD) could provide early microstructural alterations in Alzheimer's disease (AD) and suspected non-Alzheimer's pathophysiology (SNAP), but the spatial and temporal patterns of cMD and their associations with AD and SNAP have been poorly investigated.
2. **Interpretation**: Elevated cMD levels are more sensitive to detecting brain structural alterations than cortical thinning and gray matter atrophy in cognitively impaired older adults. Cortical tau aggregations and age-related white matter hyperintensity mainly drive cMD increases in AD and SNAP, respectively.

   Tau- and vascular disease–related elevated cMD levels partially explain the amyloid beta–related and fully mediated age-related cognitive impairment longitudinal cognitive decline in AD and SNAP, respectively. These findings may assist in tracking earlier neurodegenerative processing in AD and SNAP patients.
3. **Future directions**: It would be helpful to validate these findings in other independent cohorts with more sensitive cortical microstructural indicators.

2.3 | PET imaging and analysis

Details about FBP, FBB, and FTP image acquisition and analysis are provided at https://adni.loni.usc.edu/. Briefly, PET data were acquired in 4 × 5-minute frames from 50 to 70 minutes for FBP, 90 to 110 minutes for FBB, and 75 to 105 minutes (6 × 5-minute frames) for FTP post-injection. PET images were then motion corrected, realigned to a standard image, then averaged into one static frame, and the averaged images were filtered to produce images of a uniform isotropic resolution of 6 mm FWHM. The fully pre-processed PET scans were downloaded from the Laboratory of Neuro Imaging (LONI) website in May 2023. All PET scans were co-registered with their T1 MRI scans that were closest in time to PET scans. Sixty-eight FreeSurfer-defined ROIs were used to extract reginal FBP, FBB, and FTP measurements from the co-registered PET scans as described previously.[27]

Cross-sectional FBP or FBB standardized uptake value ratios (SUVRs) were calculated by dividing an AD-summarized cortical area (including frontal, cingulate, parietal, and temporal regions) uptake value to that in the whole cerebellum to generate the summary COMPOSITE SUVR. In this study, COMPOSITE SUVR for FBP ≥ 1.11 or FBB ≥ 1.08 were defined as A+, as described previously.[27] The COMPOSITE FBP and FBB SUVRs were converted to Centiloids

using the equations Centiloid = (196.9 × $SUVR_{FBP}$) − 196.03 and Centiloid = (159.08 × $SUVR_{FBB}$) − 151.65, respectively.

For FTP, the composite temporal-metaROI (including entorhinal, amygdala, parahippocampal, fusiform, inferior temporal, and middle temporal regions) SUVR was calculated using inferior cerebellar gray matter intensity normalization in native MRI space.[28]

2.4 | Vascular risk factors

Based on ADNI's vascular risk factor data, we selected hyperlipidemia (HLD), hypertension (HTN), and diabetes. To define HLD, HTN, and diabetes as present (+) or absent (−), we searched text fields within the participants' self-reported medical history (RECM-HIST.csv and INITHEALTH.csv files downloaded from the LONI website on August 21, 2023) using the following criteria to define the presence of these risk factors: HLD: "hyperlipidemia" or "cholesterol"; HTN: "hypertension" or "HTN" or "high blood pressure"; and diabetes: "diabete." Cases in which "w/o HTN" was noted were classified as HTN−. Diabetes was excluded from the analyses due to the limited sample size.

2.5 | Cognitive assessments

Previously validated Preclinical Alzheimer Cognitive Composite (PACC) score was used to represent global cognition in this study, as we explained in our previous study.[29]

2.6 | Statistical analysis

All statistical analyses were performed using statistical program R (v. 4.2.2, the R Foundation for Statistical Computing). The normality of distribution was tested using the Shapiro-Wilk test in this study. Unless otherwise specified, the demographics were presented as the median and interquartile range (IQR) for continuous characteristics or number (No.) and percentage (%) for categorical characteristics. The characteristics at baseline of A−/CU, A−/CI, A+/CU, and A+/CI groups were compared using a Mann–Whitney *U* test for continuous characteristics or Fisher exact test for categorical characteristics. A false discovery rate (FDR) 0.05 using Benjamini–Hochberg (BH) was used for multiple comparisons correction. Linear mixed effect (LME) models were used to calculate slopes of PACC (ΔPACC), cMD (ΔcMD), CTh (ΔCTh), GMV (ΔGMV), and WMH (ΔWMH) over time based on the corresponding longitudinal dataset, including a random slope and intercept, and additionally adjusting education for ΔPACC.

Generalized linear models (GLMs) were used to compare cross-sectional and longitudinal changes of cMD, CTh, and GMV among A−/CU, A−/CI, A+/CU, and A+/CI groups based on 68 FreeSurfer-defined ROIs, controlling for age, sex, apolipoprotein E (*APOE*) ε4 status, and 12 kinds of DWI protocols used in this study. We defined individuals with at least one ε4 allele as *APOE* ε4 carriers and individuals without ε4 allele as *APOE* ε4 non-carriers. The ROIs with the largest *t* values in A−/CI and A+/CI individuals compared to the A−/CU group were identified, and the hierarchical cluster analysis was used to identify the ROIs among the largest *t* values into the top cMD increases cluster, which was defined as the cMD-metaROI for A−/CI and A+/CI individuals.

To explore how Aβ plaque and tau tangles relate to micro- and macro-structural changes in A−/CU, A−/CI, A+/CU, and A+/CI individuals, we investigated the associations of baseline and slopes of cMD, CTh, and GMV with cortical Aβ PET Centiloid and tau PET SUVR using Model 1, controlling for age, sex, *APOE* ε4 status, and DWI protocols.

Model 1: *baseline/slopes of cMD/CTh/GMV ~ Aβ PET + tau PET + Age + Sex + APOE ε4 + Protocols*

Subsequently, we determined how vascular risk factors, age, and sex relate to baseline and slopes of cMD, CTh, and GMV using Model 2.

Model 2: *baseline/slopes of cMD/CTh/GMV ~ WMH + HLD + HTN + Age + Sex + APOE ε4 + Protocols*

Finally, we investigated the association of Aβ PET Centiloid, tau PET SUVR, cMD-metaROI cMD, and ΔPACC using the GLM model. The sequential association of Aβ PET, tau PET, cMD-metaROI cMD, and ΔPACC in the A+ group was explored using latent variable modeling (R, Lavaan package), controlling for age, sex, protocols, and education as covariates. Similarly, the association of age, WMH, cMD-metaROI cMD, and ΔPACC and their sequential association were also investigated in the A- group, controlling for sex, protocols, and education as covariates. Additionally, we compared baseline cMD, CTh, and GMV and the cross-sectional association of cMD with Aβ, tau, age, and WMH in individuals with longitudinal data.

3 | RESULTS

3.1 | Demographics

The demographic characteristics of participants in this study are summarized in Table 1. At baseline, among 617 participants, 305 (51%) were females, 296 (48%) were A+, 303 (49%) were CI, and the median age was 72.4 years (IQR 10.3 years, range: 55.2 to 93.5 years). Compared to the reference A−/CU group, the A−/CI ($P = 0.005$), A+/CU ($P < 0.001$), and A+/CI ($P < 0.001$) groups were older, the CI group had a higher percentage of males ($P < 0.001$), and the A+ group had a higher percentage of *APOE* ε4 carriers ($P < 0.001$), as well as significantly higher Aβ PET Centiloids ($P < 0.001$). The comparisons of ages and percentages of females, A+, CI, and *APOE* ε4 in 383 individuals with tau PET scans had similar demographic characteristics. The characteristics of longitudinal data with cMD, WMH, and PACC scores are also illustrated in Table 1. The median visit of DWI was 3 (IQR 2, range: 2 to 13), with a median duration time of 2.2 (IQR 2.2, range: 0.4 to 11.0 years). The demographic characteristics at the baseline of participants with and without longitudinal participants were similar. The details of their comparisons were summarized in Tables S1-S3 in supporting information.

TABLE 1 Demographics of participants.

	A−/CU	A−/CI	A+/CU	A+/CI
617 participants with concurrent Aβ PET and DWI at baseline				
No. patients (%)	219 (35.5)	102 (16.5)	95 (15.4)	201 (32.6)
Age, years	69.3 (7.8)	73.0 (11.9)[a]	73.7 (9.0)[b]	74.6 (9.2)[c]
Female, no. (%)	134 (61.2)	34 (33.3)[a,d]	64 (67.4)	80 (39.8) [c,f]
*APOE ε*4 carrier, no. (%)	57 (26.0)	26 (25.5)	49 (51.6)[b,d]	143 (71.1)[c,e,f]
Aβ PET Centiloids	2.8 (12.2)	1.0 (15.6)	47.3 (46.8)[b,d]	90.2 (54.5)[c,e,f]
PACC scores	0.8 (3.6)	−4.7 (5.5)[a,d]	0.0 (4.2)	−10.8 (10.0)[c,e,f]
Hypertension, no. (%)	88 (40.2)	60 (58.8)[a]	47 (49.5)	99 (49.3)
Hyperlipidemia, no. (%)	99 (45.2)	60 (58.8)[a]	52 (54.7)	103 (51.2)
421 participants with concurrent Aβ PET and longitudinal DWI, T2 FLAIR and PACC score				
No. patients (%)	139 (33.0)	78 (18.5)	56 (13.3)	148 (35.2)
Age, years	70.0 (8.2)	73.1 (10.2)[a]	73.6 (7.3)[b]	74.5 (9.0)[c]
Female, no. (%)	83 (59.7)	23 (29.5)[a,d]	37 (66.1)	60 (40.5)[c,f]
Visits of DWI (points)	3 (2, 2–9)	3 (3, 2–13)	3 (1, 2–9)	3 (2, 2–10)
Duration of DWI (years)	3.6 (2.8, 0.4–10.2)	3.0 (2.5, 0.5–11.0)	2.1 (2.3, 0.6–9.8)	2.0 (2.0, 0.5–9.3)
382 participants with concurrent Aβ PET, tau PET, and DWI at baseline				
No. patients (%)	157 (41.1)	60 (16.7)	69 (18.0)	96 (25.1)
Age, years	67.9 (7.0)	73.4 (13.4)[a]	73.7 (8.3)[b]	75.2 (9.7)[c]
Female, no. (%)	102 (65.0)	23 (38.3)[a,d]	43 (62.3)	38 (39.6)[c,f]
*APOE ε*4 carrier, no. (%)	40 (25.5)	12 (20.0)	40 (58.0)[b,d]	66 (68.8)[c,e]
Aβ PET Centiloids	3.2 (10.8)	2.1 (12.4)	49.4 (47.9)[b,d]	92.3 (48.7)[c,e,f]
tau PET SUVR	1.2 (0.1)	1.2 (0.1)	1.2 (0.1) [b,d]	1.5 (0.5)[c,e,f]
PACC scores	0.8 (2.9)	−4.6 (5.0)[a,d]	0.4 (3.5)	−10.6 (10.0)[c,e,f]
Hypertension, no. (%)	54 (34.4)	35 (58.3)[a]	33 (47.8)	47 (49.0)
Hyperlipidemia, no. (%)	67 (42.7)	39 (65.0)[a]	42 (60.9)[b]	52 (54.2)
211 participants with concurrent longitudinal DWI, T2 FLAIR and PACC score				
No. patients (%)	83 (39.3)	36 (17.1)	35 (16.6)	57 (27.0)
Age, years	68.4 (8.6)	74.1 (13.3)[a]	73.7 (7.9)[b]	74.6 (9.4)[c]
Female, no. (%)	57 (69)	10 (28)[a,d]	20 (57)	24 (42)[c]
Visits of DWI (points)	2 (1, 2–4)	2 (1, 2–5)	2 (1, 2–4)	3 (1, 2–5)
Duration of DWI (years)	2.3 (2.0, 1.0–4.6)	2.0 (1.9, 0.9–4.6)	2.0 (2.2, 1.0–4.3)	2.0 (1.7, 0.9–4.0)

Note. Data are presented as number of participants (no.) and percentage (%) or median and interquartile range (IQR). Benjamini–Hochberg was used for group-level multiple corrections (significant level, $P < 0.05$).

[a]A−/CI versus A−/CU.
[b]A+/CU versus A−/CU.
[c]A+/CI versus A−/CU.
[d]A+/CU versus A−/CI.
[e]A+/CI versus A−/CI.
[f]A+/CI versus A+/CU.

Abbreviations: Aβ, amyloid beta; *APOE*, apolipoprotein E; CI, cognitively impaired; CU, cognitively unimpaired; DWI, diffusion-weighted imaging; FLAIR, fluid-attenuated inversion recovery; PACC, Preclinical Alzheimer Cognitive Composite; PET, positron emission tomography; ROI, region of interest; SUVR, standardized uptake value ratio; WMH, white matter hyperintensity

3.2 | Comparison of micro- and macro-structural changes among different stages of dementia

Compared to the A−/CU group, A−/CI individuals had significant cMD increases in quite broad areas of the brain, including bilateral insula, parahippocampal, anterior cingulate, isthmus cingulate, and lateral and medial orbitofrontal regions (Figure 1A), but showed significant CTh and GMV decreases primarily in the entorhinal, parahippocampal, and middle temporal regions (Figure 1C, E). In addition, A+/CI individuals showed significantly more cMD increases and CTh and GMV decreases

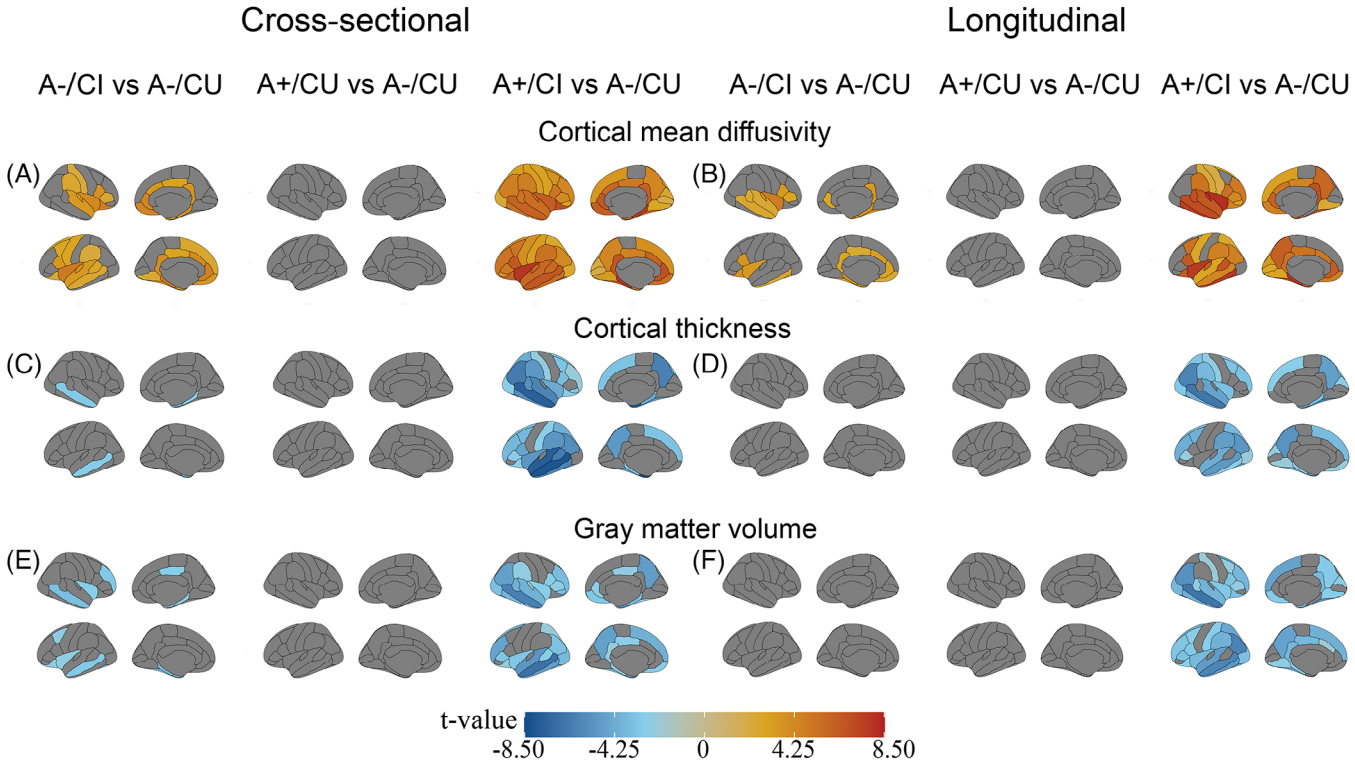

FIGURE 1 Cross-sectional and longitudinal microstructural and macrostructural changes among different Aβ PET positivity and clinical stages. Comparison of baseline levels and slopes of (A-B) cortical mean diffusivity, (C-D) cortical thickness, and (E-F) gray matter volume in the A−/CU group with (A) the A+/CI and (B) A/CI groups. Notably, A− = Aβ PET negative; A+ = Aβ PET positive. Aβ, amyloid beta; CI, cognitively impaired; CU, cognitively unimpaired; PET, positron emission tomography

in many overlapped regions than the A−/CU group, although cMD had the most affected regions, followed by CTh, and GMV had the least affected regions. Longitudinally, A−/CI individuals showed faster cMD increases in cingulate and temporal regions (Figure 1B), but no significant regions were found for decreased CTh and GMV compared to the A−/CU individuals (Figure 1D, F). The A+/CI individuals showed significantly faster cMD increases, CTh declines, and GMV decreases in substantial overlapped regions. No significant difference was found between A+/CU and A−/CU individuals, regardless of cross-sectional and longitudinal comparisons in cMD, CTh, and GMV.

Compared to the A−/CU group, the hierarchical cluster analysis identified that A−/CI individuals showed the highest cMD increases in the parahippocampal, insula, and rostral anterior cingulate cortices (Figure 2B) and, additionally, isthmus cingulate for the A+/CI individuals (Figure 2A). In the following analysis, we defined the above four ROIs as the cMD-metaROI (Figure 2C) for evaluating the cMD change. As shown in Figure 3, approximately 2- and 3-fold larger effect sizes between A−/CI and A−/CU groups were observed in cross-sectional and longitudinal cMD increases of cMD-metaROI than CTh and GMV decreases of temporal-meROI. Furthermore, the comparisons in baseline levels and slopes of cMD within cMD-metaROI between A+/CI and A−/CU group had much larger effect sizes than in CTh and GMV decreases of temporal-metaROI as well as cMD-metaROI (Figure S1 in supporting information).

3.3 | Prediction of cMD, CTh, and GMV by Aβ PET and tau PET

Cross-sectionally, elevated cMD levels in multiple brain regions were negatively associated with Aβ PET in the A−/CI group, whereas they positively related to tau PET in the A+/CI group (Figure 4A-B). Longitudinally, tau PET but not Aβ PET was associated with faster rates of cMD increases in bilateral inferior temporal, middle temporal, banks of the superior temporal sulcus, cingulate, and precuneus regions in the A+/CI group (Figure 4C-D), but no other significant relation was found. In line with the 68 ROIs analysis, we found that Aβ PET was negatively related to baseline cMD level of cMD-metaROI (Figure 5A, standardized β [β_{std}] = −0.286 [95% confidence interval: −0.511, −0.061], P = 0.016) in A−/CI individuals, whereas tau PET was positively associated with cross-sectional (Figure 5C, β_{std} = 0.405 [95% confidence interval: 0.187, 0.622], $P < 0.001$) and longitudinal (Figure 5D, β_{std} = 0.436 [95% confidence interval: 0.141, 0.731], P = 0.005) cMD increases of cMD-metaROI in A+/CI individuals. Meanwhile, we investigated the association of CTh and GMV with Aβ PET and tau PET (Figures S2 and S3 in supporting information). In A+/CI individuals, cross-sectional and longitudinal decreases of CTh and GMV, primarily in the temporal lobe, were negatively correlated with tau PET but not with Aβ PET, but the associated regions were less than cMD. Cross-sectional comparisons for baseline cMD, CTh, and GMV in individuals

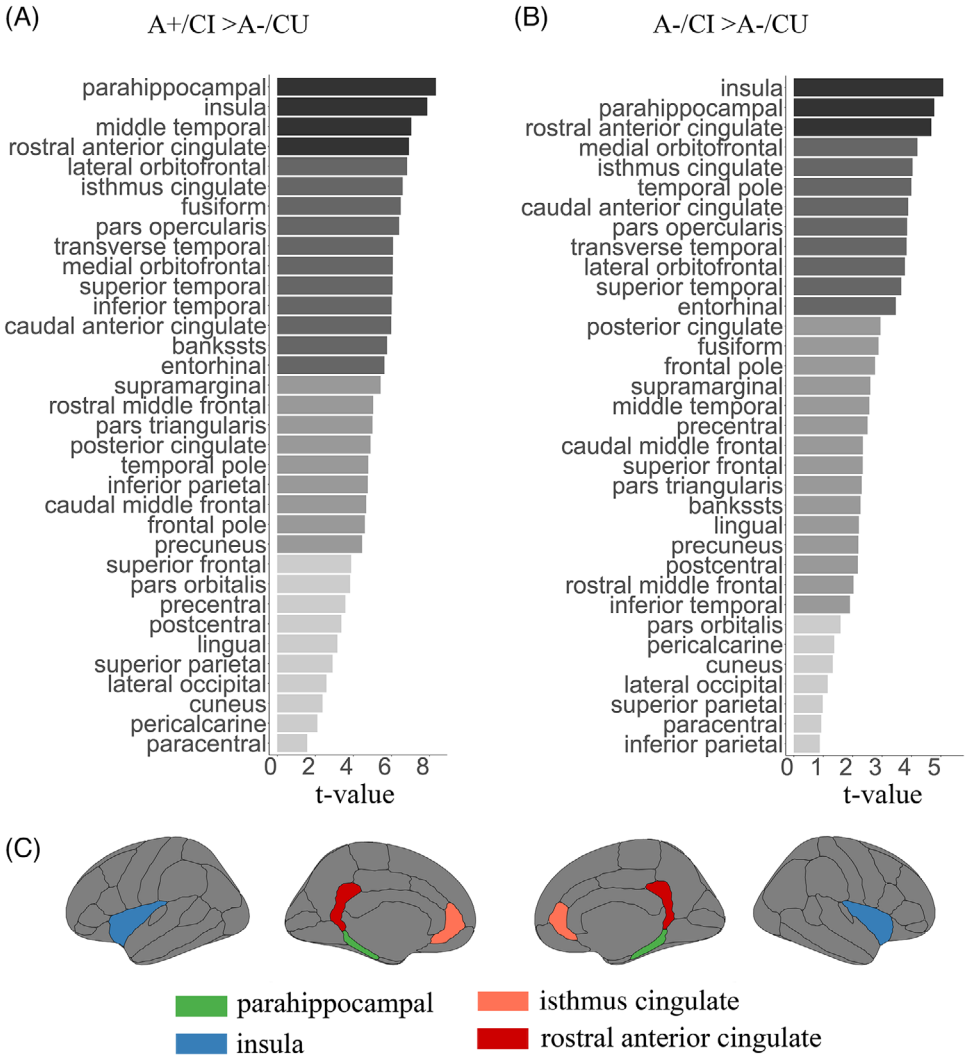

FIGURE 2 The hierarchical cluster analysis defined cMD-metaROI regions of cognitively impaired individuals. The comparisons of cortical mean diffusivity in the A−/CU group with (A) the A+/CI and (B) A−/CI groups. C, The illustration of hierarchical cluster analysis defined cMD-metaROI regions of CI individuals. Notably, A− = Aβ PET negative; A+ = Aβ PET positive. CI, cognitively impaired; cMD, cortical mean diffusivity; CU, cognitively unimpaired; PET, positron emission tomography; ROI, region of interest

with longitudinal data substantially showed similar results (Figure S4 in supporting information). The negative association disappeared in the Aβ− CI subgroup with concurrent Aβ PET and longitudinal DWI, T2 FLAIR, and PACC score (Figure S5A in supporting information).

3.4 | Prediction of cMD, CTh, and GMV by age and vascular risk factors

Baseline cMD levels were positively associated with older ages in A−/CU, A−/CI, and A+/CU groups but not in the A+/CI group and related to higher WMH mainly in the A−/CU, A−/CI, and A+/CI groups (Figure 6). Longitudinally, older ages predicted faster rates of cMD increases in the cMD-metaROI as well as middle temporal and inferior temporal regions in the A− group but not in the A+ group, and larger WMH correlated with faster rates of cMD increases in the cMD-metaROI and inferior temporal regions in A−/CU. Additionally, males had higher cMD than females in several cortical areas, for example, cMD-metaROI in the A+/CU group and supramarginal and superior frontal in the A+/CI group (Figure S6 in supporting information). Similarly, we also found significant age-related baseline CTh and GMV decreases in A−/CU and A−/CI individuals (Figure S7 and Figure S8 in supporting information). In contrast, no relationship was found between cMD, CTh, and GMV and HLD, HTN, and *APOE* ε4 status.

3.5 | Association of cMD and longitudinal cognitive decline in Aβ− individuals and AD patients

Among 321 A- individuals, older ages were positively correlated with larger WMH (Figure S9A in supporting information; $\beta_{std} = 0.397$ [95% confidence interval: 0.269, 0.526], $P < 0.001$) and cMD (Figure S9B;

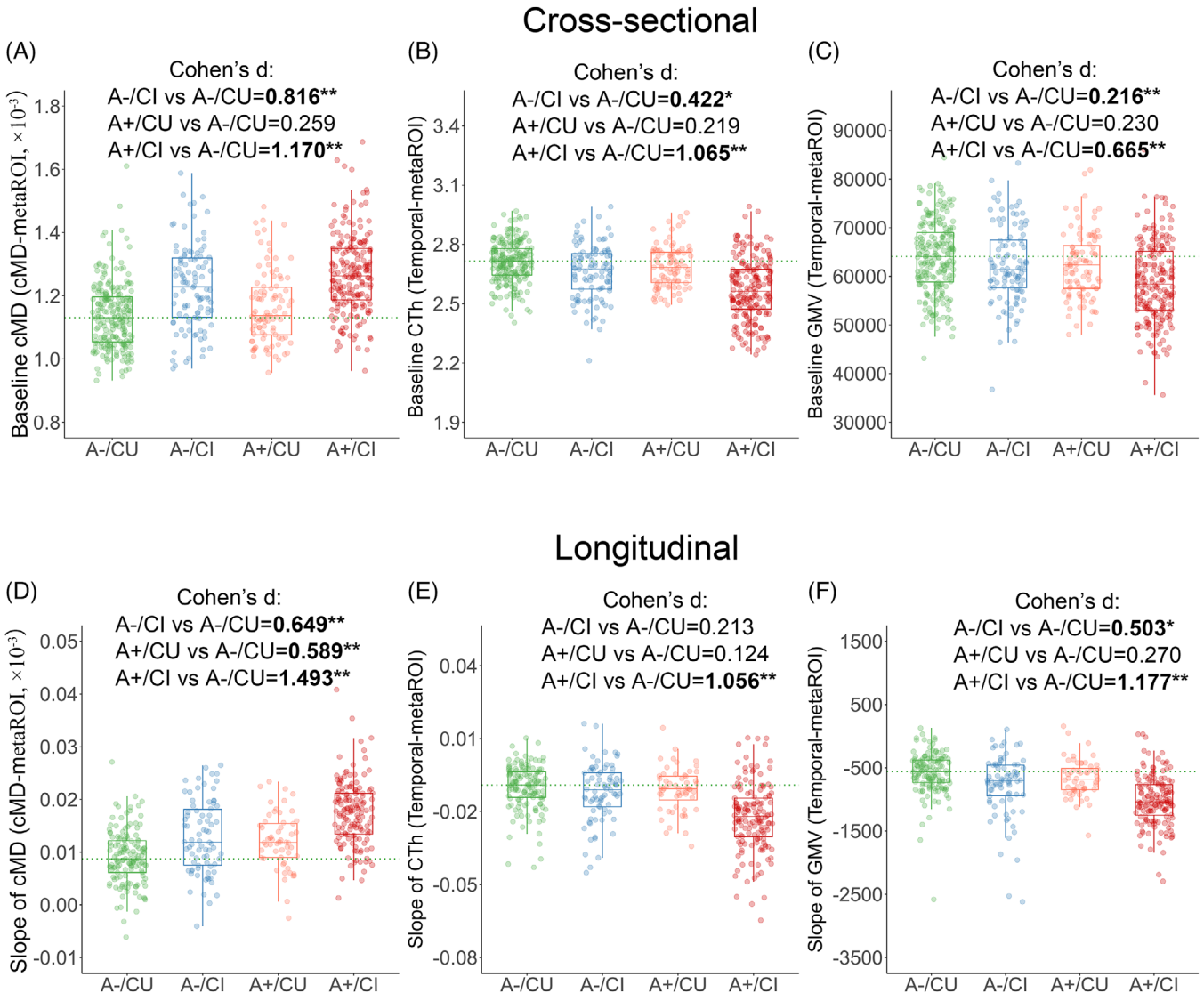

FIGURE 3 Comparison of cMD-metaROI cortical mean diffusivity and temporal-metaROI cortical thickness and gray matter volume among different Aβ PET positivity and clinical stages. Comparisons of baseline levels and slopes of (A, D) cMD-metaROI cortical mean diffusivity, (B, E) temporal-metaROI cortical thickness, and (C, F) temporal-metaROI gray matter volume between A−/CU, A−/CI, A+/CU, and A+/CI groups. Notably, A− = Aβ PET negative; A+ = Aβ PET positive. Aβ, amyloid beta; CI, cognitively impaired; cMD, cortical mean diffusivity; CU, cognitively unimpaired; PET, positron emission tomography; ROI, region of interest

β_{std} = 0.558 [95% confidence interval: 0.471, 0.645], $P < 0.001$), and negatively related to faster PACC decline (Figure S9C; β_{std} = −0.224 [95% confidence interval: −0.353, −0.095], $P < 0.001$). Among 165 A+ participants with tau PET scans, Aβ PET Centiloids were positively correlated with tau PET SUVR (Figure S9D; β_{std} = 0.512 [95% confidence interval: 0.378, 0.645], $P < 0.001$) and cMD increases (Figure S9E; β_{std} = 0.281 [95% confidence interval: 0.140, 0.423], $P < 0.001$), and negatively related to faster rates of PACC decline (Figure S9F; β_{std} = −0.482 [95% confidence interval: −0.638, −0.327], $P < 0.001$). Finally, we investigated the sequential association of age, WMH, cMD, and ΔPACC in A− individuals and the association of Aβ PET, tau PET, cMD, and ΔPACC in A+ individuals. Among A− individuals, higher WMH-related cMD fully mediated the relation between age and longitudinal cognitive decline, which explained 89.6% ([−0.031+(−0.098)]/[−0.144] = 0.896) of the association between age and ΔPACC (Figure 7A). In contrast, tau-associated cMD increases only partially mediated the association between Aβ PET and longitudinal cognitive decline in A+ individuals. Increased tau and tau-associated cMD explained 64.5% ([−0.084+(−0.423)]/[−0.786] = 0.645) and 10.7% (−0.084/[−0.786] = 0.107) of the relation between Aβ and ΔPACC (Figure 7B), respectively.

4 | DISCUSSION

In this study, we investigated cross-sectional and longitudinal microstructural (cMD) and macrostructural (CTh and GMV) alterations as well as how they correlate with age, vascular risk factors,

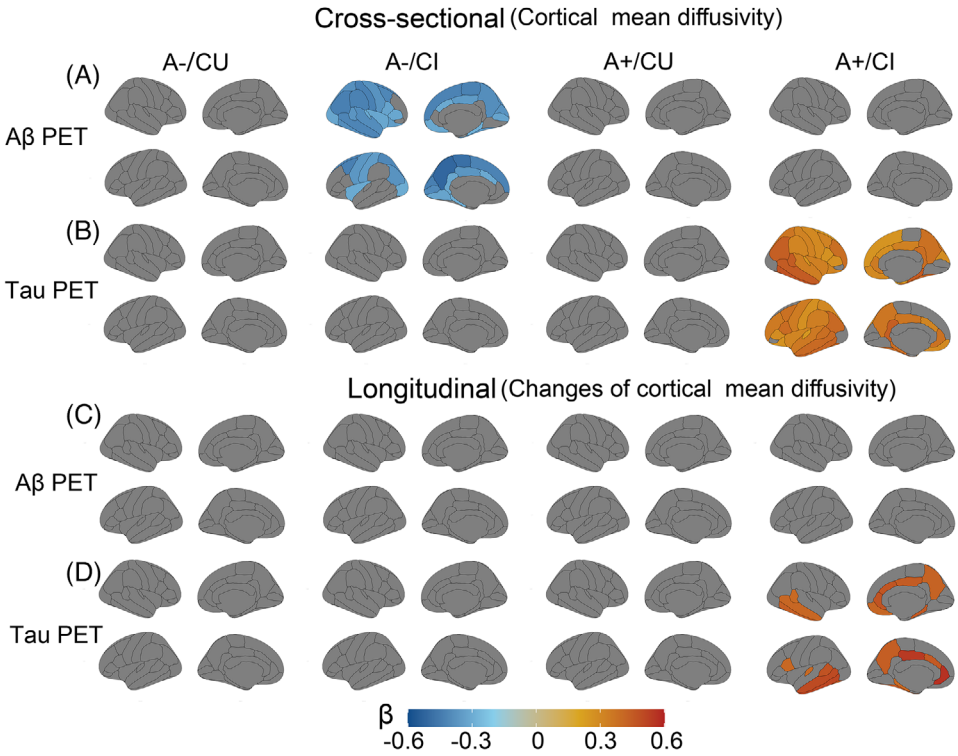

FIGURE 4 Association of cortical mean diffusivity with Aβ PET and tau PET. Association of baseline levels and slopes of cortical mean diffusivity in 68 FreeSurfer-defined regions with (A, C) Aβ PET Centiloid and (B, D) tau PET SUVR in A−/CU, A−/CI, A+/CU, and A+/CI groups. Notably, A− = Aβ PET negative; A+ = Aβ PET positive. Aβ, amyloid beta; CI, cognitively impaired; CU, cognitively unimpaired; PET, positron emission tomography

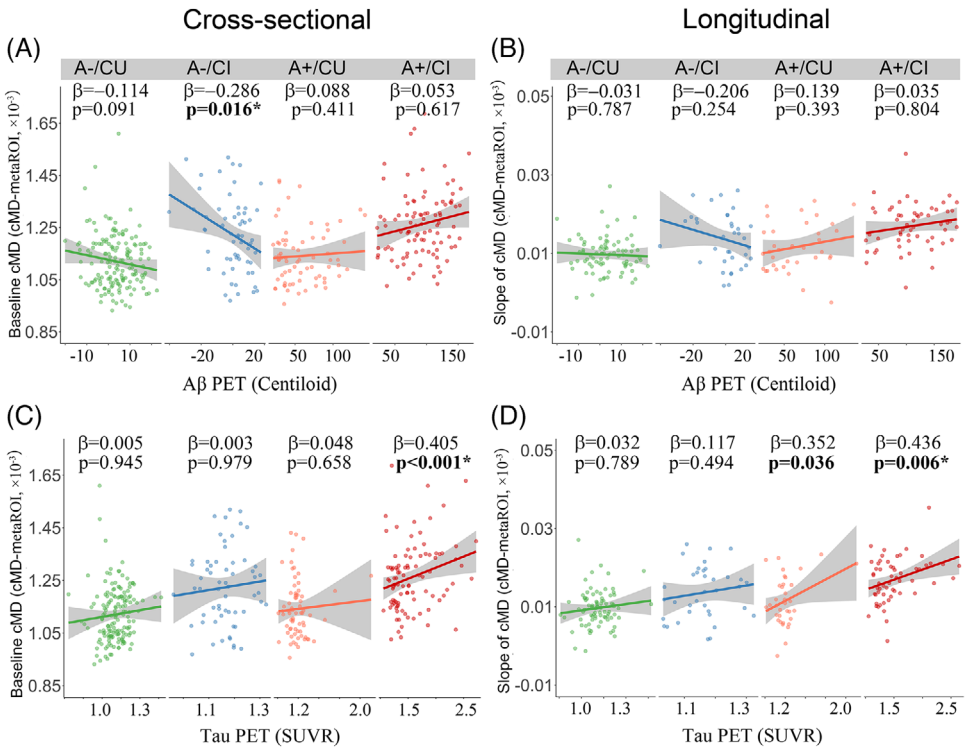

FIGURE 5 Association of cMD-metaROI cortical mean diffusivity with Aβ PET and tau PET. Association of baseline levels and slopes of cMD-metaROI cMD with (A, C) Aβ PET Centiloid and (B, D) tau PET SUVR in A−/CU, A−/CI, A+/CU, and A+/CI groups. Notably, A− = Aβ PET negative; A+ = Aβ PET positive. Aβ, amyloid beta; CI, cognitively impaired; cMD, cortical mean diffusivity; CU, cognitively unimpaired; PET, positron emission tomography; ROI, region of interest; SUVR, standardized uptake value ratio

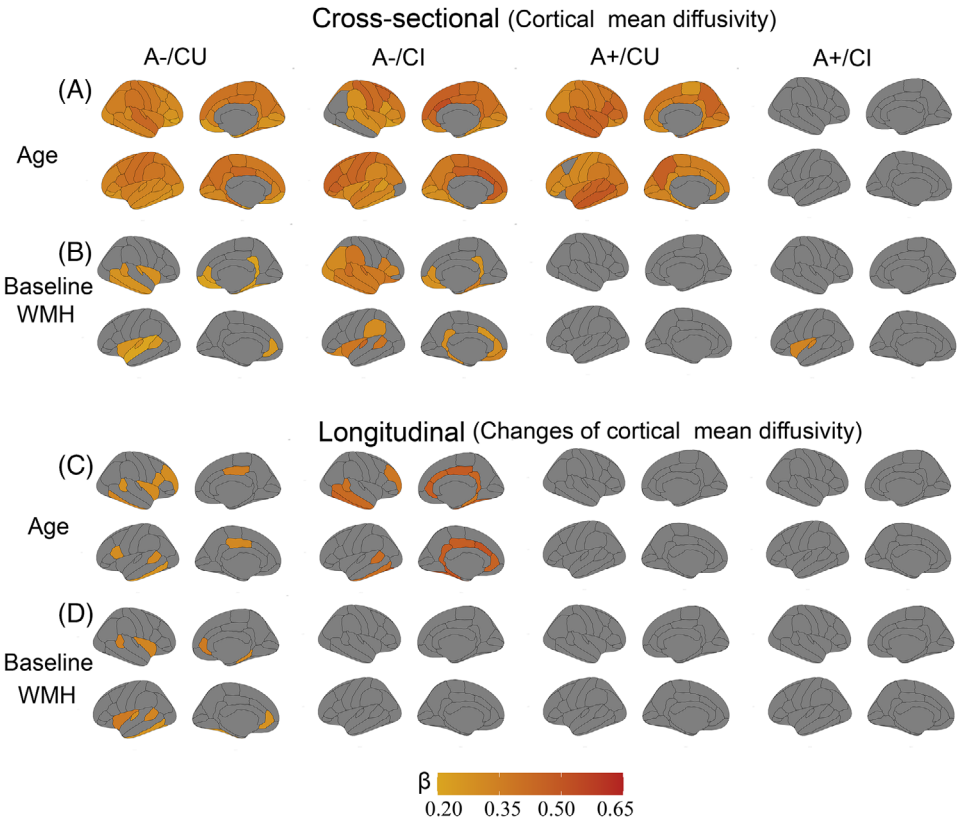

FIGURE 6 Cross-sectional and longitudinal association of cortical mean diffusivity with age and white matter hyperintensities. Association of (A-B) baseline levels and (C-D) longitudinal changes of cortical mean diffusivity with age and white matter hyperintensities in A−/CU, A−/CI, A+/CU, and A+/CI groups. Notably, A− = Aβ PET negative; A+ = Aβ PET positive. Aβ, amyloid beta; CI, cognitively impaired; CU, cognitively unimpaired; PET, positron emission tomography; WMH, white matter hyperintensity

Aβ plaque, tau tangles, and longitudinal cognitive decline in Aβ PET–negative and -positive older adults. We found that cMD increases are more sensitive to detecting brain structural alterations than cortical thinning and gray matter atrophy in older adults with cognitive impairment, particularly in Aβ PET–negative individuals. Significant cMD increases were observed in the parahippocampal, insula, isthmus cingulate, and rostral anterior cingulate regions (cMD-metaROI) regardless of Aβ positivity. Furthermore, tau PET SUVRs were strongly linked to cross-sectional and longitudinal increases of cMD in Aβ PET–positive CI individuals, indicating that the Aβ-related cognitive decline was only partially due to tau-associated cMD increases. In Aβ PET–negative individuals, in contrast, older ages and greater WMH were associated with cross-sectional and longitudinal cMD increases, suggesting that cMD increase is a downstream effect of aging and part of the association between aging and cognitive decline is mediated by cMD increases. These findings revealed the dynamic changes of microstructural and macrostructural imaging indicators and their associations with age, vascular risk factors, AD pathologies, and cognitive decline, providing novel insights into understanding upstream and downstream events of cMD in AD and SNAP patients.

One of the primary findings of this study was that increased cMD seems more sensitive and robust to detecting abnormal structural changes than cortical thinning and gray matter atrophy in CI individuals, particularly in Aβ− individuals. Consistent with our findings, previous studies reported that cMD may capture subtle microstructural changes antedating gray matter atrophy.[18,30] In addition, one study proposed that microstructural changes precede changes in macrostructure.[19] Unlike previous studies,[19,31] we did not observe significant cMD increases or decreases in preclinical AD individuals compared to the Aβ PET–negative CU group. The former study[19] found significantly decreased cMD in preclinical CSF Aβ positive and CSF phosphorylated tau (p-tau)–negative individuals, whereas the latter one[31] observed significant cMD increases in CSF Aβ positive and CSF p-tau–negative non-demented individuals compared to the control group. The earlier positivity of CSF Aβ compared to Aβ PET[32] and the different extraction locations of MD may explain the discrepancy. Nevertheless, the present study found no significant decreases in CTh and GMV in preclinical AD individuals compared to the Aβ PET–negative CU older adults, which aligned with the microstructural findings. Together, these results indicate that significant neurodegeneration reflected by microstructural increases or macrostructural decreases may be detectable in CI individuals but not in preclinical AD, but microstructural alterations show more robustness than cortical thinning and gray matter atrophy, especially in Aβ− individuals.

Among CI older adults, the hierarchical cluster analysis identified a composite cMD-metaROI region, consisting of parahippocampal,

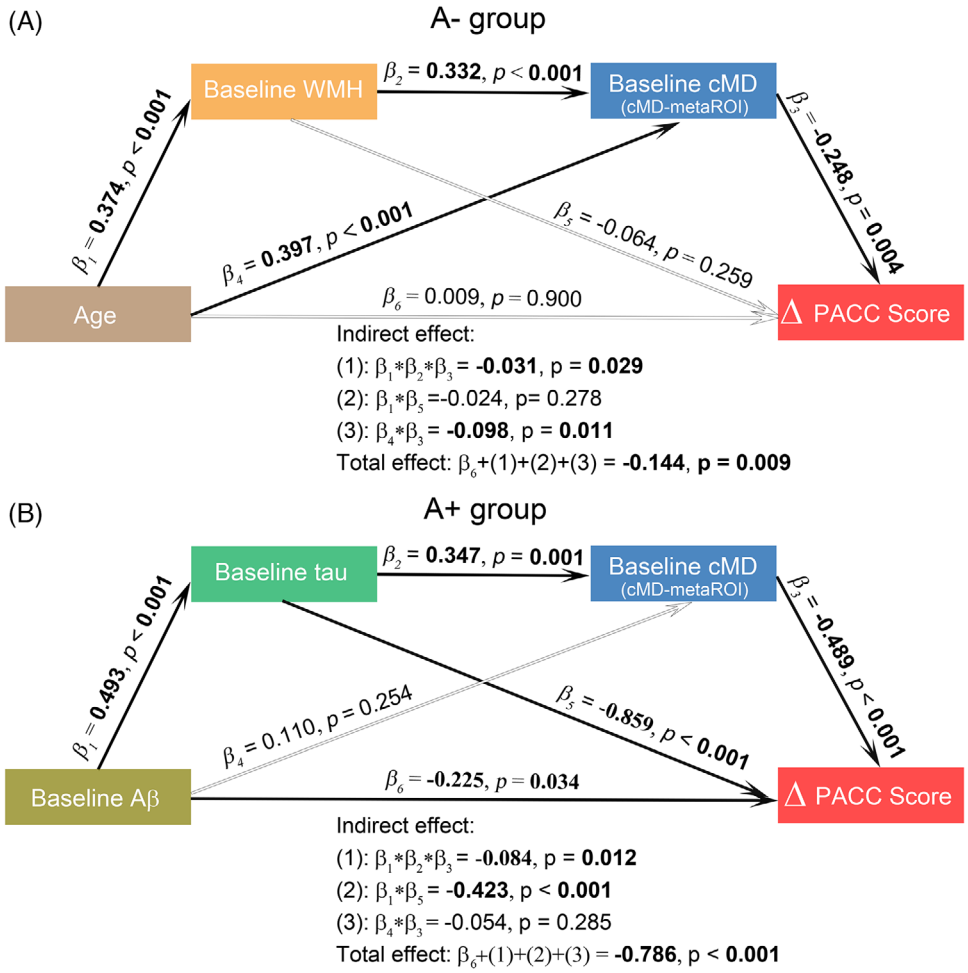

FIGURE 7 Association of cortical mean diffusivity with age, WMHs, Aβ, tau, and longitudinal decline. A, The mediation analysis of age, WMHs, cMD-metaROI cMD, and longitudinal changes of PACC (ΔPACC) in Aβ PET negative individuals, and (B) the association of Aβ PET, tau PET, cMD-metaROI cMD, and ΔPACC in Aβ PET positive individuals. Aβ, amyloid beta; CI, cognitively impaired; CU, cognitively unimpaired; PACC, Preclinical Alzheimer Cognitive Composite; PET, positron emission tomography; ROI, region of interest; WMH, white matter hyperintensity

insula, isthmus cingulate, and rostral anterior cingulate cortices, with the highest cMD levels. Given the critical role of the limbic system involved in processing memories, emotions, and other cognitive functions,[33] previous studies reported that the limbic network shows early adaptation in subjective cognitive decline individuals irrespective of Aβ pathology[34] and breakdown in clinical variants of AD,[35] age-related memory impairments,[36] and SNAP patients.[37] Notably, recent viral infection studies suggest that the limbic system and associated brain structures[38] are involved in inflammatory response,[39,40] and neuroinflammation is related to microglial activation in AD.[31] Microglial activation distributes preferentially along highly connected brain regions, similar to tau pathology.[41,42] A recent study on white matter neuroinflammation also confirms its association with AD pathologies and cognition.[43] Additionally, the parahippocampus is a subregion of the medial temporal lobe, which is crucial for episodic memory.[38,44] Besides the limbic network, the insula and cingulate cortex are also two critical hubs of the salience network, responding to attention-grabbing and guiding behavior in response to stimuli,[45] which is proven to be vulnerable in AD[46] and SNAP.[47,48] Previous network and connectivity studies mainly focus on white matter degeneration[49] or cortical macrostructural changes. Notably, one proof-of-concept study suggests that cMD might reflect underlying neuroinflammatory mechanisms in the early stages of AD.[50] Also, another study provides an association between cMD and longitudinal changes of fluid markers reflecting astrocytic activity (i.e., the plasma level of glial fibrillary acidic protein and CSF levels of YKL-40).[31] Our defined cMD-metaROI also included the cortical regions examined in the two aforementioned studies, which correlated with neuroinflammation. Further studies are critical to exploring the limbic system's association with inflammation. Together, the cMD increases of the cMD-metaROI region may be one of the significant indicators for abnormal cortical microstructural alterations in AD and SNAP.

Cortical tau tangle but not Aβ plaque aggregations were strongly associated with cross-sectional and longitudinal cMD increases, cortical thinning, and gray matter atrophy in Aβ PET–positive CI individuals but not in other groups. This implies that tau tangles are more related to microstructural and macrostructural alterations than Aβ plaques in AD patients, consistent with the previous AD cohort studies.[14,22,51,52]

Critically, the present study further demonstrated that tau-related cMD increases appear in a more extensive brain area, including the cingulate, precuneus, and temporal lobe, compared to the cortical thinning and gray matter atrophy in AD. Specifically, tau-associated cortical thinning and gray matter atrophy were observed in relatively limited brain regions, providing additional evidence that microstructural alterations may be more sensitive to reflect tau-related neurodegeneration than cortical thinning and brain atrophy. Unexpectedly, we found that Aβ plaques were negatively related to cMD increases in Aβ− CI individuals, although significantly larger cMD were observed in Aβ− CI individuals compared to the A−/CU individuals. Further investigation will be essential to elucidate the mechanism underlying this phenomenon. In addition, one recent study did not find a significant association between tau and fractional anisotropy in white matter,[53] indicating microstructural changes in white matter and gray matter may represent different aspects of microstructural degeneration. Altogether, tau-associated cMD increases show a promising potential of detecting brain structural alterations compared to white matter microstructural alterations, cortical thinning, and gray matter atrophy in AD.

Our group has demonstrated that older ages are associated with vascular disease and SNAP.[15] The multivariable regression analysis of the present study further found that older ages correlated with higher baseline cMD levels and faster rates of cMD increase in the Aβ PET−negative older adults regardless of cognitive impairment. We[54] and other groups[55,56] recently observed that older ages are correlated with more significant WMH burdens. This study showed a significant correlation between WMH and cMD in Aβ PET−negative individuals cross-sectionally and longitudinally. Furthermore, the mediation analysis revealed that the cognitive decline of Aβ− individuals was substantially explained by the elevated cMD levels, probably due to the older ages or age-related WMH increases. In line with our results, previous studies also reported that DTI model-based parameters in gray matter were associated with age[57] and WMH.[58] These findings suggest that aging and cerebrovascular risk factors in Aβ PET−negative individuals may be linked to cMD increases, and such an increase in cMD partially mediated the association of aging and vascular risk factors with longitudinal cognitive decline. However, in AD patients, tau was irrefutable as the foremost factor predicting faster cognitive decline compared to the cMD, which is consistent with the recent perspective that effects of Aβ on neurodegeneration and cognitive decline are fully mediated by tau in the genetically identical twin-pair study.[59]

In this study, we analyzed a large dataset with cross-sectional and longitudinal T1 MRI and DWI images using the accurate surface-based method[19] to investigate the dynamic changes of cMD, CTh, and GMV and their relationships with AD and non-AD individuals. These findings are beneficial for understanding the longitudinal microstructural and macrostructural alterations and provide novel references for tracking earlier neurodegeneration in AD and non-AD patients. However, this study has several limitations. First, to the best of our knowledge, the ADNI cohort has the most comprehensive concurrent Aβ PET, tau PET, T2-FLAIR, and longitudinal T1 MRI and DWI image data at this moment, but validating these findings using independent datasets is critical and would be extremely helpful in the future, particularly for the association between Aβ PET and cMD in Aβ PET−negative CI individuals. Second, technical limitations for the DTI-based cMD parameter should be considered for cortical microstructural change detection. Future studies with high-resolution DWI approaches are expected to validate these findings. Third, recent studies have shown that models with higher b-values, for example, neurite orientation dispersion and density imaging (NODDI)[17] and mean apparent propagator MRI,[60] are more sensitive to detecting early neurodegeneration in AD and SNAP patients compared to the cMD indicator. However, it is essential to note that cMD still provides comparable patterns with AD pathologies as the NODDI approach,[61] and cMD owns the advantages of quick acquisition and clinical penetration.

In summary, this study demonstrates that cMD increases may detect more sensitive brain structural alterations than cortical thinning and gray matter atrophy in AD and Aβ PET−negative CI individuals. Furthermore, cortical tau aggregations mainly drive cMD increases, partially explaining the Aβ-related longitudinal cognitive decline in the AD continuum. These findings provide novel insights into understanding the spatial and temporal patterns of microstructure and macrostructure as well as their association with age, vascular disease, Aβ plaque, and tau tangles in Aβ PET−negative and -positive older adults, which may assist in tracking earlier neurodegenerative signs in AD and non-AD patients.

ACKNOWLEDGMENTS

The authors thank all the ADNI participants and staff for contributing to data acquisition. The image processing was supported by the Shenzhen Bay Laboratory supercomputing center. This study was funded by the Guangdong Basic and Applied Basic Science Foundation for Distinguished Young Scholars (Grant No. 2023B1515020113), the Shenzhen Science and Technology Program (Grant No. RCYX20221008092935096), the National Natural Science Foundation of China (Grant No. 82171197), Shenzhen Bay Laboratory (Grant No. S241101004-1, 21300061), and the Lingang Laboratory (Grant No. LG-GG-202401-ADA070600).

CONFLICT OF INTEREST STATEMENT

The authors declare no competing interests. Author disclosures are available in the supporting information.

CONSENT STATEMENT

The ADNI study was approved by institutional review boards of all participating institutions, and written informed consent was obtained for ethical considerations.

ORCID

Tengfei Guo https://orcid.org/0000-0003-2982-0865

REFERENCES

1. Hansson O, Blennow K, Zetterberg H, Dage J. Blood biomarkers for Alzheimer's disease in clinical practice and trials. *Nat Aging*. 2023;3:506-519. doi:10.1038/s43587-023-00403-3

2. Guo T, Dukart J, Brendel M, Rominger A, Grimmer T, Yakushev I. Rate of β-amyloid accumulation varies with baseline amyloid burden: implications for anti-amyloid drug trials. *Alzheimer's Dement*. 2018;14:1387-1396. doi:10.1016/j.jalz.2018.05.013
3. Cai Y, Du J, Li A, et al. Initial levels of β-amyloid and tau deposition have distinct effects on longitudinal tau accumulation in Alzheimer's disease. *Alzheimers Res Ther*. 2023;15:30. doi:10.1186/s13195-023-01178-w
4. Jack CR, Bennett DA, Blennow K, et al. NIA-AA Research Framework: toward a biological definition of Alzheimer's disease. *Alzheimer's Dement*. 2018;14:535-562. doi:10.1016/j.jalz.2018.02.018
5. Jack CR, Knopman DS, Chételat G, et al. Suspected non-Alzheimer disease pathophysiology-concept and controversy. *Nat Rev Neurol*. 2016;12:117-124. doi:10.1038/nrneurol.2015.251
6. Young CB, Winer JR, Younes K, et al. Divergent cortical tau positron emission tomography patterns among patients with preclinical Alzheimer disease. *JAMA Neurol*. 2022;79:592. doi:10.1001/jamaneurol.2022.0676
7. Mattsson-Carlgren N, Andersson E, Janelidze S, et al. Aβ deposition is associated with increases in soluble and phosphorylated tau that precede a positive Tau PET in Alzheimer's disease. *Sci Adv*. 2020;6:eaaz2387. doi:10.1126/sciadv.aaz2387
8. Lowe VJ, Lundt ES, Albertson SM, et al. Neuroimaging correlates with neuropathologic schemes in neurodegenerative disease. *Alzheimer's Dement*. 2019;15:927-939. doi:10.1016/j.jalz.2019.03.016
9. Ozlen H, Pichet Binette A, Köbe T, et al. Spatial extent of amyloid-β levels and associations with Tau-PET and cognition. *JAMA Neurol*. 2022;79:1025. doi:10.1001/jamaneurol.2022.2442
10. van der Kall LM, Truong T, Burnham SC, et al. Association of β-amyloid level, clinical progression, and longitudinal cognitive change in normal older individuals. *Neurology*. 2021;96:e662-e670. doi:10.1212/WNL.0000000000011222
11. Chen X, Toueg TN, Harrison TM, Baker SL, Jagust WJ. Regional tau deposition reflects different pathways of subsequent neurodegeneration and memory decline in cognitively normal older adults. *Ann Neurol*. 2023;1:731-737. doi:10.1002/ana.26813
12. Wisse LEM, de Flores R, Xie L, et al. Pathological drivers of neurodegeneration in suspected non-Alzheimer's disease pathophysiology. *Alzheimers Res Ther*. 2021;13:100. doi:10.1186/s13195-021-00835-2
13. Oberstein TJ, Schmidt MA, Florvaag A, et al. Amyloid-β levels and cognitive trajectories in non-demented pTau181-positive subjects without amyloidopathy. *Brain*. 2022;145:4032-4041. doi:10.1093/brain/awac297
14. Guo T, Korman D, Baker SL, Landau SM, Jagust WJ. Longitudinal cognitive and biomarker measurements support a unidirectional pathway in Alzheimer's disease pathophysiology. *Biol Psychiatry*. 2021;89:786-794. doi:10.1016/j.biopsych.2020.06.029
15. Guo T, Landau SM, Jagust WJ. Age, vascular disease, and Alzheimer's disease pathologies in amyloid negative elderly adults. *Alzheimers Res Ther*. 2021;13:174. doi:10.1186/s13195-021-00913-5
16. Weston PSJ, Simpson IJA, Ryan NS, Ourselin S, Fox NC. Diffusion imaging changes in grey matter in Alzheimer's disease: a potential marker of early neurodegeneration. *Alzheimer's Res Ther*. 2015;7:1-8. doi:10.1186/s13195-015-0132-3
17. Vogt NM, Hunt JF, Adluru N, et al. Cortical microstructural alterations in mild cognitive impairment and Alzheimer's disease dementia. *Cereb Cortex*. 2020;30:2948-2960. doi:10.1093/cercor/bhz286
18. Illán-Gala I, Montal V, Pegueroles J, et al. Cortical microstructure in the amyotrophic lateral sclerosis-frontotemporal dementia continuum. vol. 95. 2020. doi:10.1212/WNL.0000000000010727
19. Montal V, Vilaplana E, Alcolea D, et al. Cortical microstructural changes along the Alzheimer's disease continuum. Alzheimer's. *Dement*. 2018;14:340-351. doi:10.1016/j.jalz.2017.09.013
20. Montal V, Bejanin A, Vilaplana E, et al. Biphasic cortical macro- and microstructural changes in autosomal dominant Alzheimer ' s disease 2020:1-11. doi:10.1002/alz.12224
21. Ding W, Ren P, Yi L, et al. Association of cortical and subcortical microstructure with disease severity: impact on cognitive decline and language impairments in frontotemporal lobar degeneration. Alzheimer's. *Res Ther*. 2023;15:1-24. doi:10.1186/s13195-023-01208-7
22. Rodriguez-Vieitez E, Montal V, Sepulcre J, et al. Association of cortical microstructure with amyloid-β and tau: impact on cognitive decline, neurodegeneration, and clinical progression in older adults. *Mol Psychiatry*. 2021;26:7813-7822. doi:10.1038/s41380-021-01290-z
23. Archer DB, Schilling K, Shashikumar N, et al. Leveraging longitudinal diffusion MRI data to quantify differences in white matter microstructural decline in normal and abnormal aging. *Alzheimer's Dement Diagnosis, Assess Dis Monit*. 2023;15:1-13. doi:10.1002/dad2.12468
24. Hong H, Tozer DJ, Markus HS. Relationship of perivascular space markers with incident dementia in cerebral small vessel disease. *Stroke*. 2024:1032-1040. doi:10.1161/strokeaha.123.045857
25. Jack CR, Wiste HJ, Weigand SD, et al. Defining imaging biomarker cut points for brain aging and Alzheimer's disease. *Alzheimer's Dement*. 2017;13:205-216. doi:10.1016/j.jalz.2016.08.005
26. Liang L, Zhou P, Lu W, et al. An anatomical knowledge-based MRI deep learning pipeline for white matter hyperintensity quantification associated with cognitive impairment. *Comput Med Imaging Graph Off J Comput Med Imaging Soc*. 2021;89:101873. doi:10.1016/j.compmedimag.2021.101873
27. Jiang C, Wang Q, Xie S, et al. β-Amyloid discordance of cerebrospinal fluid and positron emission tomography imaging shows distinct spatial tau patterns. *Brain Commun*. 2022;4. doi:10.1093/braincomms/fcac084
28. Du J, Li A, Shi D, et al. Association of APOE -ε4, osteoarthritis, β-amyloid, and tau accumulation in primary motor and somatosensory regions in Alzheimer disease. *Neurology*. 2023;101:e40-e49. na
29. Guo T, Korman D, La Joie R, et al. Normalization of CSF pTau measurement by Aβ40 improves its performance as a biomarker of Alzheimer's disease. *Alzheimers Res Ther*. 2020;12:97. doi:10.1186/s13195-020-00665-8
30. Ganepola T, Nagy Z, Ghosh A, Papadopoulo T, Alexander DC, Sereno MI. Using diffusion MRI to discriminate areas of cortical grey matter. *Neuroimage*. 2018;182:456-468. doi:10.1016/j.neuroimage.2017.12.046
31. Spotorno N, Strandberg O, Stomrud E, et al. Diffusion MRI tracks cortical microstructural changes during the early stages of Alzheimer's disease. *Brain*. 2024;147:961-969. doi:10.1093/brain/awad428
32. Guo T, Shaw LM, Trojanowski JQ, Jagust WJ, Landau SM. Association of CSF Aβ, amyloid PET, and cognition in cognitively unimpaired elderly adults. *Neurology*. 2020;95:e2075-e2085. doi:10.1212/WNL.0000000000010596
33. Rolls ET. The cingulate cortex and limbic systems for emotion, action, and memory. *Brain Struct Funct*. 2019;224:3001-3018. doi:10.1007/s00429-019-01945-2
34. Jiang X, Hu X, Daamen M, et al. Altered limbic functional connectivity in individuals with subjective cognitive decline: converging and diverging findings across Chinese and German cohorts. *Alzheimer's Dement*. 2023;19:4922-4934. doi:10.1002/alz.13068
35. Pini L, Wennberg AM, Salvalaggio A, Vallesi A, Pievani M, Corbetta M. Breakdown of specific functional brain networks in clinical variants of Alzheimer's disease. *Ageing Res Rev*. 2021;72:101482. doi:10.1016/j.arr.2021.101482
36. Bender AR, Brandmaier AM, Düzel S, et al. Hippocampal subfields and limbic white matter jointly predict learning rate in older adults. *Cereb Cortex*. 2020;30:2465-2477. doi:10.1093/cercor/bhz252

37. Nelson PT, Dickson DW, Trojanowski JQ, et al. Limbic-predominant age-related TDP-43 encephalopathy (LATE): consensus working group report. *Brain*. 2019;142:1503-1527. doi:10.1093/brain/awz099
38. de Flores R, Das SR, Xie L, et al. Medial temporal lobe networks in Alzheimer's disease: structural and molecular vulnerabilities. *J Neurosci*. 2022;42:2131-2141. doi:10.1523/JNEUROSCI.0949-21.2021
39. Guedj E, Morbelli S, Kaphan E, et al. From early limbic inflammation to long COVID sequelae. *Brain*. 2021;144:10-12. doi:10.1093/brain/awab215
40. Thomasson M, Voruz P, Cionca A, et al. Markers of limbic system damage following SARS-CoV-2 infection. *Brain Commun*. 2023;5:1-11. doi:10.1093/braincomms/fcad177
41. Rauchmann B, Brendel M, Franzmeier N, et al. Microglial activation and connectivity in Alzheimer disease and aging. *Ann Neurol*. 2022;92:768-781. doi:10.1002/ana.26465
42. Passamonti L, Tsvetanov KA, Jones PS, et al. Neuroinflammation and functional connectivity in Alzheimer's disease: interactive influences on cognitive performance. *J Neurosci*. 2019;39:7218-7226. doi:10.1523/JNEUROSCI.2574-18.2019
43. Wang Q, Schindler SE, Chen G, Mckay NS, Investigating White Matter Neuroin fl ammation in Alzheimer Disease Using Di ff usion-Based Neuroin fl ammation Imaging 2024:1-13. doi:10.1212/WNL.0000000000208013
44. Berron D, van Westen D, Ossenkoppele R, Strandberg O, Hansson O. Medial temporal lobe connectivity and its associations with cognition in early Alzheimer's disease. *Brain*. 2020;143:1233-1248. doi:10.1093/brain/awaa068
45. Cormie MA, Kaya B, Hadjis GE, Mouseli P, Moayedi M. Insula-cingulate structural and functional connectivity: an ultra-high field MRI study. *Cereb Cortex*. 2023;33:9787-9801. doi:10.1093/cercor/bhad244
46. Gu Y, Lin Y, Huang L, et al. Abnormal dynamic functional connectivity in Alzheimer's disease. *CNS Neurosci Ther*. 2020;26:962-971. doi:10.1111/cns.13387
47. Mehraram R, Peraza LR, Murphy NRE, et al. Functional and structural brain network correlates of visual hallucinations in Lewy body dementia. *Brain*. 2022;145:2190-2205. doi:10.1093/brain/awac094
48. Du J, Zhu H, Zhou J, et al. Structural brain network disruption at preclinical stage of cognitive impairment due to cerebral small vessel disease. *Neuroscience*. 2020;449:99-115. doi:10.1016/j.neuroscience.2020.08.037
49. Qiu T, Liu Z, Rheault F, et al. Structural white matter properties and cognitive resilience to tau pathology. *Alzheimer's Dement*. 2024:1-14. doi:10.1002/alz.13776
50. Vilaplana E, Rodriguez-Vieitez E, Ferreira D, et al. Cortical microstructural correlates of astrocytosis in autosomal-dominant Alzheimer disease. *Neurology*. 2020;94:E2026-E2036. doi:10.1212/WNL.0000000000009405
51. Jack CR, Wiste HJ, Therneau TM, et al. Associations of amyloid, tau, and neurodegeneration biomarker profiles with rates of memory decline among individuals without dementia. *JAMA*. 2019;321:2316. doi:10.1001/jama.2019.7437
52. La Joie R, Visani AV, Baker SL, et al. Prospective longitudinal atrophy in Alzheimer's disease correlates with the intensity and topography of baseline tau-PET. *Sci Transl Med*. 2020;12:eaau5732. doi:10.1126/scitranslmed.aau5732
53. Cogswell PM, Lundt ES, Therneau TM, et al. Evidence against a temporal association between cerebrovascular disease and Alzheimer's disease imaging biomarkers. *Nat Commun*. 2023;14:3097. doi:10.1038/s41467-023-38878-8
54. Shi D, Xie S, Li A, et al. APOE-ε4 modulates the association among plasma Aβ42/Aβ40, vascular diseases, neurodegeneration and cognitive decline in non-demented elderly adults. *Transl Psychiatry*. 2022;12:128. doi:10.1038/s41398-022-01899-w
55. Raghavan S, Przybelski SA, Lesnick TG, et al. Vascular risk, gait, behavioral, and plasma indicators of VCID. *Alzheimer's Dement*. 2023:1-13. doi:10.1002/alz.13540
56. Eloyan A, Thangarajah M, An N, et al. White matter hyperintensities are higher among early-onset Alzheimer's disease participants than their cognitively normal and early-onset nonAD peers: longitudinal Early-onset Alzheimer's Disease Study (LEADS). *Alzheimer's Dement*. 2023;19:S89-S97. doi:10.1002/alz.13402
57. Radhakrishnan H, Bennett IJ, Stark CEL. Higher-order multi-shell diffusion measures complement tensor metrics and volume in gray matter when predicting age and cognition. *Neuroimage*. 2022;253:119063. doi:10.1016/j.neuroimage.2022.119063
58. Torso M, Bozzali M, Zamboni G, Jenkinson M, Chance SA. Detection of Alzheimer's Disease using cortical diffusion tensor imaging. *Hum Brain Mapp*. 2021;42:967-977. doi:10.1002/hbm.25271
59. Coomans EM, Tomassen J, Ossenkoppele R, et al. Genetically identical twin-pair difference models support the amyloid cascade hypothesis. *Brain*. 2023:1-6. doi:10.1093/brain/awad077
60. Spotorno N, Strandberg O, Vis G, Stomrud E, Nilsson M, Hansson O. Measures of cortical microstructure are linked to amyloid pathology in Alzheimer's disease. *Brain*. 2023;146:1602-1614. doi:10.1093/brain/awac343
61. Nir TM, Villalón-Reina JE, Salminen LE, et al. Cortical microstructural associations with CSF amyloid and pTau. *Mol Psychiatry*. 2023. doi:10.1038/s41380-023-02321-7

SUPPORTING INFORMATION

Additional supporting information can be found online in the Supporting Information section at the end of this article.

How to cite this article: Sun P, He Z, Li A, et al. Spatial and temporal patterns of cortical mean diffusivity in Alzheimer's disease and suspected non-Alzheimer's disease pathophysiology. *Alzheimer's Dement*. 2024;1-14. https://doi.org/10.1002/alz.14176